Dynamics of Dipole-Inverted *cis*-Polyisoprene Chains in a Matrix of Long, Entangling Chains. 1. Effects of Constraint Release on the Eigenmodes of the Local Correlation Function

Yumi Matsumiya, Hiroshi Watanabe,* and Kunihiro Osaki

Institute for Chemical Research, Kyoto University, Uji, Kyoto 611, Japan

Ming-Long Yao

Rheometric Scientific F.E. Ltd, 2-19-6 Yanagibashi, Taito-ku, Tokyo 111, Japan

Received January 16, 1998; Revised Manuscript Received August 11, 1998

ABSTRACT: For a series of *cis*-polyisoprene (PI) chains having nearly the same molecular weight ($M \cong 50000$) but differently once-inverted dipoles parallel along the chain backbone, dielectric behavior was examined in homogeneous blends in an entangling polybutadiene (PB) matrix with $M = 263\,000$. In the blends, the PI chains (5 vol %) were entangled only with the matrix chains. The constraint release (CR) mechanism made a negligible contribution to the global relaxation of those PI chains. The series of PI chains exhibited quite different dielectric losses ϵ''. These differences, reflecting the different location of the dipole inversion point in the chain backbone, were utilized to experimentally determine the eigenfunctions $f_p(n)$ and relaxation times τ_p defined for a local correlation function, $C(n,t;m) = (1/a^2)\langle \mathbf{u}(n,t)\cdot\mathbf{u}(m,0)\rangle = (2/N)\sum_p f_p(n)\, f_p(m) \exp(-t/\tau_p)$ with $\mathbf{u}(n,t)$ being the bond vector for the nth segment at time t. The $f_p(n)$ and τ_p/τ_1 ratio ($p = 1-3$) evaluated for the PI chains in the high-M PB matrix were found to be close to those determined in a low-M entangling matrix (M = 9240) as well as in the monodisperse bulk state of the same PI chains. The PI relaxation was dominated by the CR mechanism in this low-M matrix, while this mechanism made a moderate contribution to the PI relaxation in the monodisperse bulk state. Thus the close coincidence of $f_p(n)$ and the τ_p/τ_1 ratio ($p = 1-3$) in the three environments indicated that the distribution of the slowest three eigenmodes was hardly affected by the CR mechanism. In contrast, for higher eigenmodes, modest CR effects were observed through differences in the shape of the ϵ'' curves at intermediate frequencies for respective dipole-inverted PI chains in the three environments.

I. Introduction

cis-Polyisoprene (PI) chains have dipoles parallel along their backbone,[1] and their global motion induces molecular weight (M) dependent dielectric relaxation at long time scales. The PI chains have quite small dipoles and the global chain dynamics is negligibly affected by the dipole−dipole interaction. Utilizing these features, extensive dielectric studies have been carried out for PI chains in various environments such as the bulk state,[1−6] solutions,[4,7−11] and blends.[4,12−16]

The fundamental aspect of the slow dielectric relaxation of PI chains is described by a local correlation function:[6]

$$C(n,t;m) = (1/a^2)\langle \mathbf{u}(n,t)\cdot\mathbf{u}(m,0)\rangle \qquad (1)$$

Here, $\mathbf{u}(n,t)$ is a bond vector for the nth segment at time t and $a^2 = \langle \mathbf{u}^2\rangle$. (The segment size can be arbitrarily chosen according to the time scale of the dynamic phenomena of our interest.[17] This situation is similar to that for bead-spring models.) The global motion of individual PI chains, which is reflected in $C(n,t;m)$, depends on the dynamic nature of the surrounding environment.

Most of the dielectric studies so far carried out have been for r*egular* PI chains with no inversion of the dipoles.[1,2,4,5,7−9,12,16] For a regular PI chain composed of N segments, the polarization $\mathbf{P}$ is proportional to the end-to-end vector $\mathbf{R}$ and the dielectric relaxation function $\Phi(t)$ ($\equiv\langle \mathbf{P}(t)\cdot\mathbf{P}(0)\rangle/\langle \mathbf{P}^2\rangle$) is related to the local correlation function as[6]

$$\Phi(t) = \frac{\langle \mathbf{R}(t)\cdot\mathbf{R}(0)\rangle}{\langle \mathrm{R}^2\rangle} = \frac{1}{N}\int_0^N \mathrm{d}n \int_0^N \mathrm{d}m\; C(n,t;m) \qquad (2)$$

The n and m dependence of $C(n,t;m)$ is averaged in $\Phi(t)$. Thus, some details of the chain dynamics reflected in this dependence were not well-elucidated in the studies of the regular PI chains.

These details of the chain dynamics can be dielectrically examined for a series of specially designed PI chains that have identical M but differently once-inverted dipoles.[6] The structure of these chains is shown schematically in Figure 1. For a PI chain having its dipole inversion at the n^*th segment, the polarization is proportional to the difference vector $\Delta\mathbf{R} = \mathbf{R}_1 - \mathbf{R}_2$, with $\mathbf{R}_1$ and $\mathbf{R}_2$ being two end-to-center vectors (see Figure 1), and the dielectric relaxation function is related to $C(n,t;m)$ as[6]

$$\Phi(t,n^*) = \frac{1}{N}\left[\int_0^{n^*}\mathrm{d}n - \int_{n^*}^{N}\mathrm{d}n\right]\left[\int_0^{n^*}\mathrm{d}m - \int_{n^*}^{N}\mathrm{d}m\right]C(n,t;m) \qquad (3)$$

The series of dipole-inverted PI chains have the same M (N). Thus, these chains are dynamically equivalent; i.e., they have the same $C(n,t;m)$. However, $\Phi(t;n^*)$ of these chains are different because of the difference in n^*. The dielectric data from these chains can be used to *experimentally determine* the eigenfunctions $f_p(n)$ and

* To whom correspondence should be addressed.

10.1021/ma980055+ CCC: $15.00
Published on Web 09/26/1998

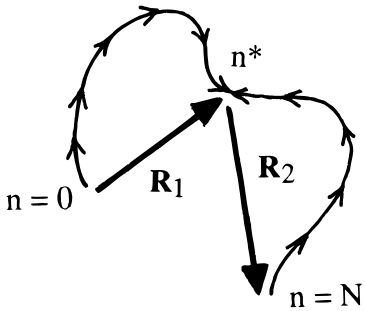

Figure 1. Schematic illustration for a dipole-inverted chain.

relaxation times τ_p defined for $C(n,t;m)$:[6]

$$C(n,t;m) = \frac{2}{N}\sum_{p=1}^{N} f_p(n) f_p(m) \exp[-t/\tau_p] \qquad (4)$$

(This symmetric form of the eigenmode expansion for C reflects the symmetry of the orientational correlation, $\langle \mathbf{u}(n,t)\cdot\mathbf{u}(m,0)\rangle = \langle \mathbf{u}(m,t)\cdot\mathbf{u}(n,0)\rangle$.[6]) The $f_p(n)$ and τ_p separately determine the n and t dependence of $C(n,t;m)$ and contain detailed information regarding the chain dynamics.

We examined the dielectric behavior of such a series of dipole-inverted PI chains and determined $f_p(n)$ and τ_p for the lowest three eigenmodes ($p = 1-3$) in the bulk state,[6] solutions,[10,11] and blends.[15] Of particular importance to the present study is the behavior of dilute, dipole-inverted PI probe chains in a matrix of much shorter, entangling polybutadiene (PB) chains.[15] The relaxation of these probe chains was induced by motion (diffusion) of the matrix PB chains. This type of *matrix-induced* relaxation mechanism is referred to as the *constraint release* (CR) mechanism.[19−21] (The CR contribution to the actual relaxation of the probe decreases with increasing matrix molecular weight and vanishes in matrices of very long chains.[22−30] In such matrices effectively working as a fixed network, the probe relaxes via its own motion, e.g., by reptation within a context of the tube model.)

The CR relaxation of the probe has been considered to proceed via retarded Rouse-like dynamics.[19−21] However, for the dipole-inverted PI probes in the short PB matrix, $f_p(n)$ is nonsinusoidal with respect to n and not explained by the Rouse-type CR model (despite a success of this model for describing the CR relaxation time).[15] To further examine the CR effects on the eigenmodes, we have investigated the dynamics of the dipole-inverted PI chains in a high-M PB matrix where the CR mechanism makes a negligible contribution to the PI relaxation. The results are presented in this series of papers.

In this paper (Part 1), $f_p(n)$ and τ_p ($p = 1-3$) are dielectrically determined for the dipole-inverted PI chains dilutely blended in the high-M PB matrix. Effects of the CR mechanism on the eigenmodes of the PI chains are examined by comparing $f_p(n)$ and τ_p for the same PI chains in the high-M and low-M entangling PB matrices as well as in the monodisperse bulk state of the PI chains themselves. (The CR contribution to the PI relaxation is different in these environments.)

The accompanying paper (Part 2)[31] addresses the relationship between dielectric and viscoelastic quantities. Specifically, the $f_p(n)$ and τ_p data obtained in this Part 1 are utilized to calculate viscoelastic moduli. Short-time coherence of the PI motion is examined in a purely experimental way through comparison of the calculated moduli and the viscoelastic data.

Table 1. Characteristics of Samples

code	$10^{-3}M_w$	M_w/M_n	n^*/N[a]
Series of Dipole-Inverted Polyisoprenes[b]			
I-I 49-0[c]	48.8	1.05	0
I-I 50-6	55.4	1.06	0.109
I-I 35-9	44.4	1.05	0.213
I-I 35-14	47.6	1.07	0.283
I-I 28-18	47.4	1.06	0.396
I-I 24-24[d]	47.7	1.06	0.5
Regular Polyisoprenes[b]			
I14	13.7	1.05	
I19	19.0	1.05	
Polybutadienes[e]			
B263	263	1.05	
B9	9.24	1.07	

[a] Reduced location of the dipole inversion point. [b] cis:trans:vinyl ≅ 75:20:5. [c] I-I 49-0, without dipole inversion, is included in this series as an extreme case of the inversion at the chain end. [d] With symmetrically inverted dipoles. [e] cis:trans:vinyl ≅ 40:50:10.

II. Experimental Section

II-1. Materials. Table 1 summarizes molecular characteristics of the dipole-inverted PI, regular PI (without dipole inversion), and PB samples used in this series of papers. All PI samples and the B9 sample were synthesized and characterized in our previous work.[6,13,15] (One of the dipole-inverted PI samples[6,10,15] was exhausted in the previous study,[15] and we here use the remaining six samples.) The dipole-inverted PI chains are composed of two PI blocks connected in a head-to-head fashion, and the dipoles are aligned in the same direction in each block but inverted at the block junction.[6] The sample code for those PI chains indicates the molecular weights of the two blocks in units of 1000. As seen in Table 1, the dipole-inverted PI chains have nearly the same M but differently inverted dipoles that are specified by the reduced location of the inversion point, n^*/N (cf. Figure 1).

The B263 sample was synthesized in this study via living anionic polymerization. Benzene and *sec*-butyllithium were used as the polymerization solvent and initiator, respectively. The molecular weight and polydispersity were determined with GPC (HLC-802UR, Tosoh) having a refractive index monitor combined with a small-angle light-scattering photometer (LS-8000, Tosoh). The microstructure was determined from NMR.

The systems subjected to dielectric measurements were homogeneous blends of the dipole-inverted PI chains in the B263 matrix. The blends were prepared by dissolving prescribed amounts of the PI and B263 samples in benzene and then allowing benzene to completely evaporate. The PI volume fraction in the blends was kept small ($\phi_{PI} = 0.05$) so that the PI chains ($M \cong 50\,000$) were not entangled among themselves.

Blends of the regular PI chains (I14 and I19) in the B263 matrix ($\phi_{PI} = 0.05$) were also prepared with the method explained above. These blends were utilized to evaluate the longest relaxation time of the dipole-inverted PI chains in this matrix.

II-2. Measurements. For the homogeneous blends of the dipole-inverted PI chains in the B263 matrix ($\phi_{PI} = 0.05$), dielectric measurements were carried out with a high-precision transformer bridge (model 1620A, QuadTech (formerly GenRad)). The dielectric cell consisted of guarded, parallel electrodes and had a vacant capacity of 120 pF. The dielectric loss ϵ'' was measured at various temperatures between 0 and 130 °C. Time−temperature superposition worked well and the ϵ'' data were reduced to a previously used reference temperature,[6,15] $T_r = 40$ °C. The B263 matrix chains had no parallel dipoles and exhibited negligibly small ϵ'' in our experimental window. Thus, the dielectric dispersions seen for the blends were exclusively attributed to the global motion of the PI chains.

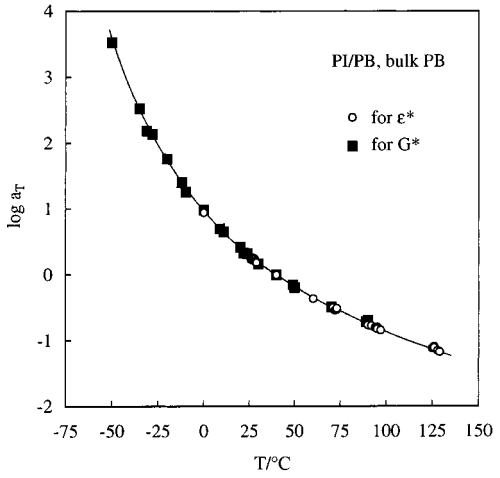

Figure 2. Temperature dependence of the shift factors for the dielectric data of dilute PI chains (with and without dipole inversion) entangled with PB matrices (unfilled circles). For comparison, the shift factors for viscoelastic moduli of I-I 49-0/B263 blend ($\phi_{PI} = 0.05$) and bulk B263 are also shown (filled squares).

For the dipole-inverted PI chains, the slowest eigenmode does not always have the largest dielectric intensity.[6,10,15] Specifically, the slowest eigenmode is dielectrically inert in the case of symmetrical dipole inversion ($n^* = N/2$; see Figure 1).[6,10,15] Thus, for those chains, the relaxation time τ_1 of the slowest eigenmode was not easily determined from their ϵ'' data, in particular when n^* was close to $N/2$. To evaluate τ_1 for the dipole-inverted chains, dielectric measurements were also carried out for blends of the regular PI chains (I14, I19, and I-I 49-0) in the B263 matrix ($\phi_{PI} = 0.05$). The ϵ'' data for these regular chains were reduced to 40 °C, and the resulting τ_1 data were interpolated/extrapolated to determine τ_1 for the dipole-inverted chains.

For the dipole-inverted and regular PI chains in the B263 matrix, good agreement was found for the shift factors $a_{T,\epsilon}$ used in the above time−temperature superposition. These $a_{T,\epsilon}$, data are shown in Figure 2. For comparison, Figure 2 also shows the shift factor $a_{T,G}$ for viscoelastic moduli G^* of the PI/B263 blends and bulk B263 matrix (cf. Part 2).[31] Excellent agreement is noted for the $a_{T,\epsilon}$ (unfilled circle) and $a_{T,G}$ (filled square). The $a_{T,\epsilon}$ represents the acceleration of the motion of the dilute PI chains in the B263 matrix with temperature, while $a_{T,G}$ essentially reflects the acceleration of the motion of the B263 chains.[13] Thus, the coincidence of $a_{T,\epsilon}$ and $a_{T,G}$ indicates that the PI and B263 chains are uniformly mixed and the segmental motion of the dilute PI chains is activated by that of the surrounding B263 chains, as also noted in a previous study.[13]

III. Results

III-1. Dielectric Behavior of Regular PI Chains in B263. In the dielectrically inert B263 matrix, each of I14, I19, and I-I 49-0 chains ($\phi_{PI} = 0.05$) exhibited a sharp ϵ'' peak immediately followed by a terminal tail ($\epsilon'' \propto \omega$) on the lower ω-side of the peak. Since these chains have no dipole inversion, the terminal dielectric mode characterized by this peak corresponds to the slowest eigenmode.[6,10,15] Thus, the relaxation time τ_1 for this eigenmode is evaluated from the angular frequency ω_{peak} at the ϵ'' peak:

$$\tau_1 = 1/\omega_{peak} \tag{5}$$

In Figure 3, these τ_1 data obtained in the B263 matrix are plotted against the PI molecular weight M_I (unfilled circles).[32] For comparison, the τ_1 data are also shown

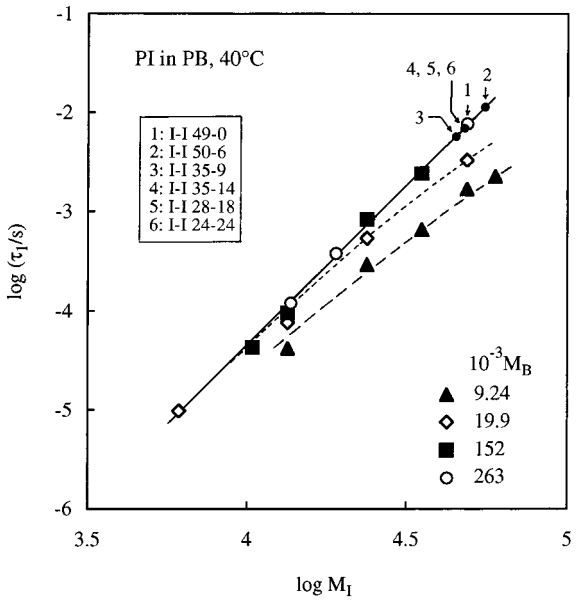

Figure 3. The longest relaxation time τ_1 of dilute PI chains (without dipole inversion) entangled with PB matrices of various molecular weights M_B as indicated (large symbols). The τ_1 data at 40 °C are plotted against the PI molecular weight M_I. The τ_1 data for $M_B = 263 \times 10^3$ were obtained in this study, and the other data were from previous work.[13,15,16] Small filled circles indicate the τ_1 of dipole-inverted PI chains calculated from an empirical equation (eq 6; shown with the solid line).

for PI chains ($\phi_{PI} \leq 0.06$) in the other entangling PB matrices examined in previous studies.[13,15]

In PI/PB blends, the PI chains are not entangled among themselves if they satisfy the criterion, $M_I < 2M_e/\phi_{PI}$, where M_e is the molecular weight between entanglements for the PI chains placed in the PB matrix ($M_e \cong 1700$ for $\phi_{PI} = 0.05$; see Part 2). (Validity of this criterion has been confirmed from the ϕ_{PI}-independence of the reduced loss ϵ''/ϕ_{PI} of dilute PI chains satisfying the criterion.[13]) All PI chains examined in Figure 3 satisfy the criterion. Thus, the τ_1 data shown there characterize the global motion of the *dilute* PI chains entangled *only with* the PB matrices.

In Figure 3, we note characteristic features for the constraint release (CR) relaxation of the PI chains: In the matrices of PB chains not much longer than the PI chains, τ_1 decreases; i.e., the global motion of the PI chains is accelerated with decreasing matrix molecular weight M_B. This acceleration is indicative of the enhanced contribution of the CR mechanism to the PI dynamics. This CR contribution becomes smaller with increasing M_B. In particular, for the PI chains with $M_I = 10\,000-50\,000$, no change of τ_1 is observed upon increasing M_B from 152 000 to 263 000. Thus the CR mechanism makes negligibly small contributions to the motion of these PI chains in the matrices with $M_B =$ 152 000 and 263 000. In these matrices, the τ_1 data for $M_I = 10\,000-50\,000$ are well-described by an empirical equation (solid line in Figure 3),

$$\tau_1/\text{s} = 7.2 \times 10^{-18} M_I^{3.2} \tag{6}$$

As explained in the Experimental Section, τ_1 of the dipole-inverted PI chains are not easily determined from their ϵ'' data, in particular, when the inversion point is close to the chain center. Thus, we used eq 6 to evaluate τ_1 of those chains. The results are shown in Figure 3 (small filled circles).

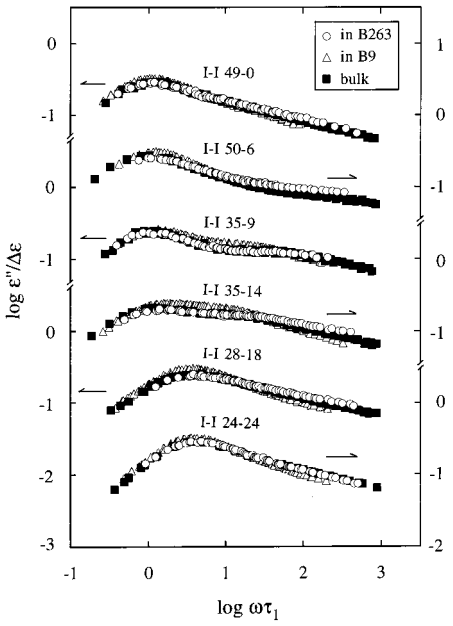

Figure 4. Frequency (ω) dependence of dielectric loss ϵ'' of dilute dipole-inverted PI chains ($\phi_{PI} = 0.05$) entangled with the B263 matrix at 40 °C (unfilled circles). For comparison, the ϵ'' data are shown for the same chains in their monodisperse bulk state[6] (filled squares) and in the B9 matrix[15] ($\phi_{PI} = 0.05$; unfilled triangles). For the best comparison of the dielectric mode distribution of the PI chains in the three environments, the ϵ'' data are reduced by the total dielectric intensity for the global chain motion $\Delta\epsilon$ and plotted against the reduced frequency $\omega\tau_1$, with τ_1 being the longest relaxation time for the local correlation function.

The above empirical equation is different from the relationship, $\tau_1 \propto M_I^3$, deduced from a conventional molecular picture of *pure* reptation[33] in very long matrices. For PI chains with M_I in the narrow range between 24 000 and 50 000, we were able to fit their τ_1 data (Figure 3) with this conventional relationship:

$$\tau_1/\mathrm{s} = 6.4 \times 10^{-17} M_I^{\,3} \qquad (7)$$

The τ_1 values for the dipole-inverted PI chains evaluated from eqs 6 and 7 were very close to each other. We thus have high confidence in these τ_1 values. (However, the difference between the power-law indices in eqs 6 and 7 raises a conceptually important problem about the probe chain dynamics in high-M matrices. This problem is discussed in Part 2.[31])

III-2. Overview of Dielectric Behavior of Dipole-Inverted PI Chains. Figure 4 shows the dielectric behavior of the dipole-inverted PI chains ($\phi_{PI} = 0.05$) in the B263 matrix at 40 °C (circles). The behavior of the same PI chains in a shorter B9 matrix ($\phi_{PI} = 0.05$)[15] and in their monodisperse bulk state ($\phi_{PI} = 1$)[6] are also shown (triangles and squares, respectively). The B263 and B9 matrices exhibited negligibly small ϵ'' at the ω examined, and the dispersions seen in Figure 4 are attributed to global motion of the PI chains. (For both PI and PB chains, the segmental motion is too fast to be detected in our ω-range.)

In the B263 and B9 matrices, the dipole-inverted PI chains (with $M_I \cong 50\,000$) satisfy the criterion for lack of entanglements among themselves, $M_I < 2M_e/\phi_{PI}$ ($M_e \cong 1700$ for $\phi_{PI} = 0.05$; see Part 2). The M_I/M_e ratio for these PI chains in the PB matrices is $M_I/M_e \cong 29$. The ratio for the same PI chains in the monodisperse bulk state is $M_I/M_e \cong 10$ ($M_e \cong 5\,000$[34,35]).

In Figure 4, the ϵ'' data are reduced by the total dielectric intensity for the global chain motion $\Delta\epsilon$ ($=(2/\pi)\int_{-\infty}^{\infty} \epsilon''\, \mathrm{d}(\ln\omega)$) and plotted against a reduced frequency $\omega\tau_1$ so that differences of ϕ_{PI} and the monomeric friction in the three environments are compensated and the dielectric mode distribution is best compared. For the dipole-inverted PI chains in the B263 matrix, the τ_1 values used in these reduced plots were determined from Figure 3. For the same chains in the B9 matrix and in the monodisperse bulk state, the τ_1 values were determined in our previous work.[6,15]

In the reduced plots, small differences in M_I of the dipole-inverted PI chains have been compensated by the factor τ_1 involved in the reduced frequency. Thus, in respective environments examined in Figure 4, we can regard the global motion of all six samples to be identical. However, the dielectric behavior is quite different because of the difference in the location of the dipole inversion point, n^*: The ϵ'' curve becomes broader and then narrower with the shift of n^* from 0 (chain end) to $N/2$ (chain center). We also note that the shape of the ϵ'' curve is almost identical for I-I 49-0 and I-I 24-24 but the ϵ'' peak is located at higher ω for the latter.[36]

The relative distribution of the slow dielectric modes is reflected in the shape of the ϵ'' curve at low ω. For PI chains having no dipole inversion, previous studies revealed that the shape is insensitive to the PI content in *concentrated* solutions,[7−10] to M_I and M_B in entangling PI/PB blends,[13,14,16] and to M_I in monodisperse bulk systems.[14,15] In Figure 4, a similar result is found for the I-I 49-0 chain: The shape of the ϵ'' curve of this chain is almost identical in the three environments. In contrast, the dipole-inverted chains having n^* between 0 and $N/2$ display modest differences in the shape of the ϵ'' curve at intermediate ω in the three environments.

III-3. Estimation of CR Contribution. In the three environments examined in Figure 4, the CR mechanism *due to the matrix motion (diffusion)* should contribute differently to the relaxation of the PI chains. To quantify this difference, we here evaluate the ratio of the characteristic time τ_{CR} for this mechanism to the observed longest relaxation time τ_1 for the I-I 49-0 chain. In matrices of long chains that exhibit very slow diffusion, I-I 49-0 relaxes via its own motion irrespective of the matrix diffusion and has $\tau_1 \ll \tau_{CR}$. On the other hand, in entangled matrices of sufficiently short chains, the relaxation is induced by the matrix diffusion and τ_1 coincides with τ_{CR}. Thus, we can use the τ_{CR}/τ_1 ratio (≥ 1) as a measure of the CR contribution to the observed relaxation of the I-I 49-0 chain: The larger the ratio, the smaller this contribution.

Extensive viscoelastic studies on binary blends of polystyrenes revealed that the relaxation of dilute probe chains (with molecular weight M_{probe}) entangled with *much shorter* matrix chains (of molecular weight M_{mat}) is governed by the CR mechanism and the τ_{CR} of such probes is proportional to $M_{probe}^2 M_{mat}^3$.[14,22−25] For dilute PI probe chains in entangling PB matrices, a previous study[13] gave an empirical equation for τ_{CR} including the proportionality constant,

$$\tau_{CR}/\mathrm{s} = 8.94 \times 10^{-25} M_I^{\,2} M_B^{\,3} \qquad (\text{at } 40\ ^\circ\mathrm{C}) \quad (8)$$

Table 2. Ratio of the CR Relaxation Time to the Observed Longest Relaxation Time for the Dilute I-I 49-0 Chain in Various Environments

matrix	τ_{CR}/τ_1
B263	5600
I-I 49-0	3.5 ± 0.3^a
B9	1.1

[a] Rough estimate for I-I 49-0 in the monodisperse bulk state.

Utilizing this equation and the τ_1 data for the I-I 49-0 chain in the B263 and B9 matrices, we evaluated the τ_{CR}/τ_1 ratio of this chain. The results are summarized in Table 2.

For *dilute* PI probes in entangling PI matrices, only a limited amount of viscoelastic/dielectric data has been reported and no accurate empirical equation of τ_{CR} is found in the literature. We here attempt to estimate the τ_{CR}/τ_1 ratio from dielectric data for the entangling PI/PI blends reported by Adachi et al.[12] They compared the τ_1 data of dilute PI probes with the prediction of a modified tube model[20] that incorporates the Rouse-type CR and pure reptation processes. The τ_{CR}/τ_1 ratio deduced from this model is written as[20]

$$\tau_{CR}/\tau_1 = 1 + [2(\pi^2/12)^z N^2/z\pi^2] \qquad (9)$$

Here, N represents the M/M_e ratio for the probe chain (with $M_e \cong 5\,000$ for bulk PI systems), and z is a parameter representing the number of topological constraints per each entanglement point for the probe chain. The τ_1 data of Adachi et al.[12] are reasonably well-described by eq 9 with $z = 3.5-4$. For the I-I 49-0 chain in its monodisperse bulk state, the τ_{CR}/τ_1 ratio evaluated from eq 9 for these z values is shown in Table 2.

The above model predicts the pure reptation behavior for the probe in matrices of very long chains. However, the I-I 49-0 chain in such a matrix (B263) does not exhibit this behavior (cf. Figure 6 shown later). Because of this difference, the τ_{CR}/τ_1 ratio obtained from eq 9 should be regarded as a rough estimate. However, this estimate is still useful for the argument below.

As seen in Table 2, the τ_{CR}/τ_1 ratio for the dilute I-I 49-0 chain is much larger than unity and very close to unity, respectively, in the B263 and B9 matrices. Thus the CR mechanism makes a negligible contribution to the global motion of I-I 49-0 in the B263 matrix (as noted also in Figure 3) while this mechanism dominates the I-I 49-0 motion in the B9 matrix (in harmony with the previous result[15]). The CR contribution for bulk I-I 49-0 lies between these two cases.

III-4. Evaluation of f_p and τ_p. The dielectric loss $\epsilon''(\omega;n^*)$ of a PI chain having the dipole inversion at the n^*th segment is given by the imaginary part of the Fourier transform of the dielectric relaxation function $\Phi(t;n^*)$ (eq 3). Considering eq 4 and carrying out this transformation, we obtain an expression for ϵ'' in terms of $f_p(n)$ and τ_p defined for $C(n,t;m)$:[6]

$$\epsilon''(\omega;n^*) = \sum_{p=1}^{N} g_p(n^*) \frac{\omega\tau_p}{1 + \omega^2\tau_p^2} \qquad (10)$$

with

$$g_p(n^*) = \Delta\epsilon[2F_p(n^*) - F_p(N)]^2 \qquad (11)$$

and

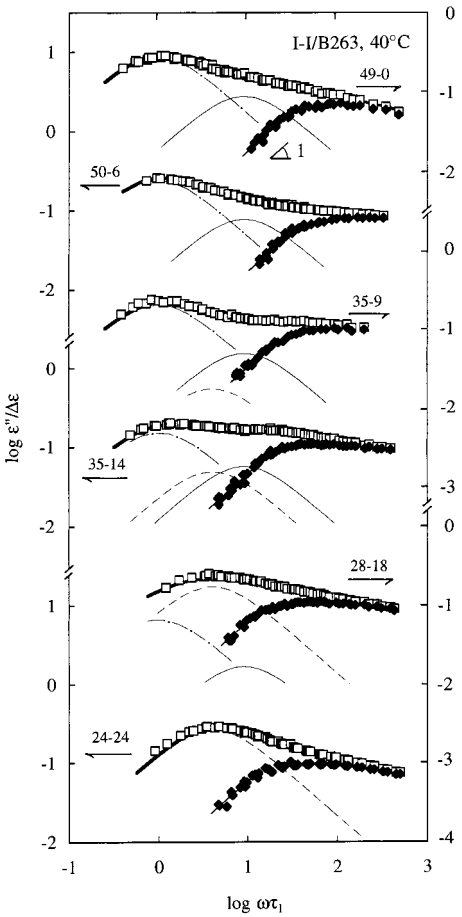

Figure 5. Decomposition of the ϵ'' data (unfilled squares) of dilute dipole-inverted PI chains ($\phi_{PI} = 0.05$) entangled with the B263 matrix at 40 °C into contributions from eigenmodes. The contributions from the slowest, second slowest, and third slowest eigenmodes are shown with the thin dash−dot, dashed, and solid curves, respectively, and the contribution from all higher (faster) eigenmodes ($p \geq 4$) is indicated with the filled diamonds. The thick solid curves indicate the sum of all these contributions.

$$F_p(n^*) = \frac{\sqrt{2}}{N}\int_0^{n^*} f_p(n)\,dn \ (=0 \text{ for } n^* = 0) \qquad (12)$$

Here, $\Delta\epsilon$ is the total dielectric intensity for the global motion of the chain, and $F_p(n^*)$ is an integrated eigenfunction. As seen in eq 11, F_p is evaluated from the intensity factor $g_p(n^*)$ for the pth dielectric mode for the PI chain having the dipole inversion at the n^*th segment. (The requirement of smooth and continuous n^* dependence of $F_p(n^*)$ as well as symmetric features of $F_p(n^*)$ are utilized in this determination.[6])

To determine the $g_p(n^*)$ values for the lowest three eigenmodes ($p = 1-3$), we here limit ourselves to low ω where the higher order eigenmodes with $p \geq 4$ have already relaxed.[37] At such low ω well-below $1/\tau_p$ for $p \geq 4$, eq 10 becomes[6]

$$\epsilon''(\omega;n^*) = \sum_{p=1}^{3} \epsilon_p''(\omega;n^*) + \omega\epsilon_{p\geq 4}^0(n^*) \qquad (13)$$

with

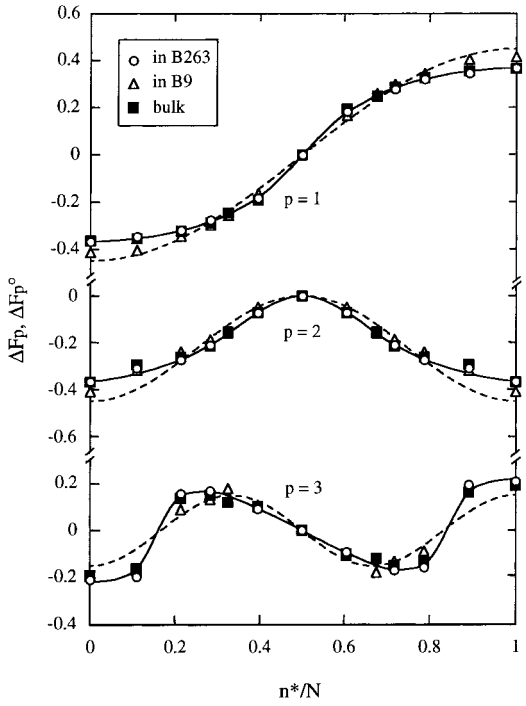

Figure 6. Dependence of integrated eigenfunctions $F_p(n^*)$ for the slowest three eigenmodes of the dilute I-I 49-0 chain (ϕ_{PI} = 0.05) entangled with the B263 matrix on the reduced segment position n^*/N (unfilled circles). For comparison, the eigenfunctions are shown for the same chain in its monodisperse bulk state[6] (filled squares) and in the B9 matrix[15] (ϕ_{PI} = 0.05; unfilled triangles). For the best comparison of the behavior of I-I 49-0 in the three environments, the plots are shown for the *base-shifted* eigenfunctions $\Delta F_p(n^*) = F_p(n^*) - F_p(N/2)$ that have a value of 0 at $n^* = N/2$ irrespective of the dynamic nature of the environment. The dashed curves indicate sinusoidal eigenfunctions commonly deduced from the pure reptation and Rouse-type CR models.

$$\epsilon_p''(\omega;n^*) = g_p(n^*)\frac{\omega\tau_p}{1+\omega^2\tau_p^2}, \quad \epsilon^0_{p\geq 4}(n^*) = \sum_{p\geq 4} g_p(n^*)\tau_p \tag{14}$$

Here, $\epsilon_p''(\omega;n^*)$ represents the contribution of the pth eigenmode to the ϵ'' data, and the term $\omega\epsilon^0_{p\geq 4}(n^*)$ indicates the low ω asymptote of the contribution from all eigenmodes with $p \geq 4$. If the $\tau_1 - \tau_3$ values are known, eq 13 becomes a linear function of the unknown quantities, $g_p(n^*)$ ($p = 1-3$) and $\epsilon^0_{p>4}(n^*)$. Then, these quantities are best determined from a linear least-squares fit of the $\epsilon''(\omega;n^*)$ data to eq 13. Details of the fitting procedure (including the optimization of the range of ω used in the fitting) were described in the previous paper.[6]

The $\tau_1 - \tau_3$ values required in this fit are determined in the following way. Since the two ends of a chain have equivalent effects on the chain motion, the eigenfunctions $f_p(n)$ should be either symmetric or antisymmetric with respect to the chain center, i.e., $f_p(n) = f_p(N-n)$ for $p = odd$ and $f_p(n) = -f_p(N-n)$ for $p = even$.[6] Because of these features of f_p, only odd eigenmodes contribute to ϵ'' for a chain having no dipole inversion ($g_p(0) = 0$ for p = even) while only even eigenmodes contribute to ϵ'' for a chain having symmetrical dipole inversion ($g_p(N/2) = 0$ for p = odd);[6] see eqs 11 and 12. Thus, the terminal dielectric mode corresponds to the slowest and second slowest eigenmodes for I-I 49-0 ($n^* = 0$) and I-I 24-24 ($n^* = N/2$), respectively. Since the ϵ'' peak of these chains is immediately followed by the terminal tail ($\epsilon'' \propto \omega$) on the low ω side (see Figure 4), the peak corresponds to the terminal dielectric mode. Thus, τ_1 and τ_2 *for I-I 49-0* are evaluated as the reciprocal of the peak frequencies for I-I 49-0 and I-I 24-24, respectively, with τ_2 being subjected to a minor correction for the small difference in M of these chains. (The correction factor is given by the ratio of the τ_1 values of those chains, where τ_1 of I-I 24-24 is determined from Figure 3.) The τ_3 value for I-I 49-0 is evaluated from a previously explained, linear least-squares analysis[6] of the ϵ'' data of this chain.

For the dilute I-I 49-0 in the B263 matrix, the above method gave

$$\tau_1 = 7.76 \times 10^{-3}\ \text{s},$$
$$\tau_2 = 1.95 \times 10^{-3}\ \text{s},\ \tau_3 = 0.854 \times 10^{-3}\ \text{s} \quad (\text{at } 40\ ^\circ\text{C}) \tag{15}$$

Utilizing these $\tau_1-\tau_3$ values in eqs 13 and 14, we carried out the linear least-squares fitting analysis of the $\epsilon''(\omega;n^*)$ data for the dipole-inverted PI chains in the B263 matrix. The results are shown in Figure 5. The contribution of the slowest three eigenmodes, $\epsilon_p''(\omega;n^*)$ with p = 1, 2, 3 (eq 14), is shown with the thin dash−dot, dashed, and solid curves, respectively. The filled diamonds indicate the contribution of the higher eigenmodes with $p \geq 4$, $\epsilon''_{p\geq 4}(\omega;n^*) = \sum_{p\geq 4}\epsilon_p''(\omega;n^*)$: This $\epsilon''_{p\geq 4}$ was obtained by subtracting ϵ_p'' with $p = 1-3$ from the data (squares). Note that $\epsilon''_{p\geq 4}(\omega;n^*)$ satisfies the prerequisite for the fit, $\epsilon''_{p\geq 4}(\omega;n^*) \rightarrow \omega\epsilon^0_{p\geq 4}(n^*) \propto \omega$ at sufficiently low ω (cf. eq 13).

Utilizing $g_p(n^*)$ ($p = 1-3$) determined from the above fit, we evaluated the integrated eigenfunctions for the I-I 49-0 chain (cf. eqs 11 and 12). In Figure 6, these functions in the B263 matrix (circles) are compared with the integrated eigenfunctions previously determined for the same chain in the B9 matrix (triangles)[15] and in the monodisperse bulk state (squares).[6] For the clearest comparison of these eigenfunctions, we have shown the base-shifted eigenfunctions $\Delta F_p(n^*) \equiv F_p(n^*) - F_p(N/2)$ that have the value 0 at $n^* = N/2$ irrespective of the environment. The dashed curves indicate sinusoidal eigenfunctions $\Delta F_p^\circ(n^*)$ commonly deduced from the reptation and Rouse-type CR models (cf. eq 18 shown later). For convenience for readers, some characteristic features of the eigenfunctions, the normalization and orthogonality, are summarized in the Appendix.

Figure 7 shows dependence of the relaxation time on the mode index p (= 1, 2, 3) for the I-I 49-0 chain in the B263 matrix (eq 15), in the B9 matrix, and in the monodisperse bulk state. The τ_p data for the latter two cases were obtained in the previous work.[6,15] The segmental friction ζ of the I-I 49-0 chains is the same in the blends with the B263 and B9 matrices, and the difference of τ_p in these blends reflects the difference of the CR contribution to the I-I 49-0 dynamics. On the other hand, ζ is different in the I-I 49-0 bulk and blend systems, and this difference also contributes to the difference of τ_p in these systems. For convenience for later comparison with models, Table 3 summarizes the τ_2/τ_1 and τ_3/τ_1 ratios that are not affected by this difference of ζ.

IV. Discussion

IV-1. CR Effects on Eigenmodes. In Figure 6, good agreement is seen for $\Delta F_p(n^*)$ in the B263 matrix

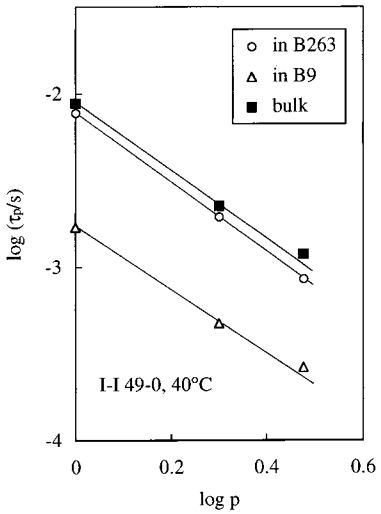

Figure 7. Dependence of the relaxation time τ_p on the eigenmode index p for the dilute I-I 49-0 chain ($\phi_{PI} = 0.05$) entangled with the B263 matrix at 40 °C (unfilled circles). For comparison, the τ_p data at 40 °C are also shown for the same chain in its monodisperse bulk state[6] (filled squares) and in the B9 matrix[15] ($\phi_{PI} = 0.05$; unfilled triangles).

Table 3. τ_2/τ_1 and τ_3/τ_1 Ratios for the Dilute I-I 49-0 Chain in Various Environments

matrix	τ_2/τ_1	τ_3/τ_1
	Observed Results	
B263	0.251	0.110
I-I 49-0[a]	0.257	0.135
B9	0.277	0.154
	Model Prediction[b]	
	0.250	0.111

[a] I-I 49-0 in the monodisperse bulk state. [b] Ratios commonly deduced from pure reptation and Rouse-type CR models.

and in the monodisperse bulk state. $\Delta F_p(n^*)$ is nearly the same also in the low-M B9 matrix, although small differences may be noted for $\Delta F_1(n^*)$ at $n^* < 0.2N$. The CR contribution to the motion of the I-I 49-0 chain is significantly different in these three environments (Table 2). Thus, we may conclude that the CR mechanism hardly affects the eigenfunctions $\Delta F_p(n)$ and $f_p(n)$ ($=\{N/\sqrt{2}\}\{d\Delta F_p(n)/dn\}$; cf. eq 12) for the *slowest three* eigenmodes.

In Figure 7, the τ_p data can be described by a power-law relationship, $\tau_p \propto p^{-\beta}$ (solid lines), in particular for I-I 49-0 in the B263 matrix (circles). The power-law index β is slightly decreased with increasing CR contribution, from $\beta = 2.0_1$ in B263 to $\beta = 1.9_8$ in the bulk state and further to $\beta = 1.8_5$ in B9 (see also Table 3). However, this decrease of β is very mild compared to the huge increase in the CR contribution (Table 2). Thus, the relaxation time spacing for $p = 1-3$ is only slightly affected by the CR contribution.

In Figure 4, we note modest differences in the shape of the ϵ'' curve for each dipole-inverted PI chain ($0 < n^* < N/2$) in the three environments. The differences are observed most clearly at intermediate ω; see, for example, the data of I-I 35-9. These differences are partly due to the small differences of the slowest three eigenmodes in those environments (e.g., the small differences in the τ_p/τ_1 ratio). However, the shape of the ϵ'' curve at intermediate ω is more strongly affected by the higher eigenmodes ($p \geq 4$), and the shape differences are expected to be essentially due to differences in these higher eigenmodes. This expectation is examined below.

In Figure 5, the dielectric loss $\epsilon''_{p\geq 4}$ due to the higher eigenmodes ($p \geq 4$) is shown with the filled diamonds. The relative contribution of these eigenmodes to the ϵ'' data is specified by the ratio, $\epsilon''_{p\geq 4}/\epsilon''$. At intermediate ω where the ϵ'' curves exhibit modestly different shapes in the three environments, the $\epsilon''_{p\geq 4}/\epsilon''$ ratio was found to increase with increasing CR contribution to the PI dynamics. For example, for the I-I 35-9 and 35-14 chains in the B263 (CR-free) and B9 (CR-dominant) matrices, the $\epsilon''_{p\geq 4}/\epsilon''$ ratio at a representative frequency, $\omega = 10/\tau_1$, is

$$\epsilon''_{p\geq 4}/\epsilon'' = 0.25\text{(I-I 35-9)}, 0.27\text{ (I-I 35-14)} \quad \text{in} \quad \text{B263} \tag{16}$$

$$\epsilon''_{p\geq 4}/\epsilon'' = 0.49\text{ (I-I 35-9)}, 0.44\text{ (I-I 35-14)} \quad \text{in} \quad \text{B9} \tag{17}$$

(These ratios were evaluated from the $\epsilon''_{p\geq 4}$ and ϵ'' data reported in this and previous[15] papers.)

The above results strongly suggest that the functional form of $f_p(n)$ and the relaxation time spacing (τ_p/τ_1 ratio) for the higher eigenmodes ($p \geq 4$) change with the CR contribution. Nevertheless, the shape of the ϵ'' curve for I-I 49-0 is almost identical in the three environments and is hardly affected by the changes in the higher eigenmodes (Figure 4). This result is related to the fact that only a half of the eigenmodes (i.e., odd eigenmodes) contribute to the ϵ'' of I-I 49-0 and the intensities of those modes, $g_p(0)$ (cf. eq 11), rapidly decrease with increasing p (because $f_p(n)$ oscillates with n more frequently for larger p). Due to this rapid decrease, the ϵ'' of I-I 49-0 seen in our experimental window is largely unaffected by the changes in the higher eigenmodes. The situation is similar for I-I 24-24: For this case, only even eigenmodes contribute to ϵ'' and their intensities ($g_p(N/2)$; cf. eq 11) decrease rapidly with increasing p, thereby giving an almost identical shape to the ϵ'' curve in the three environments (cf. Figure 4).

In summary, the CR mechanism has only a minor effect on the distribution of the slowest three eigenmodes (τ_p/τ_1 ratio and the functional form of f_p) but the effect is enhanced for higher eigenmodes. This result, which was conjectured in our previous study,[15] has now been confirmed from the comparison of the ϵ'' data of the PI chains in the CR-free and CR-dominant environments (B263 and B9 matrices). It may be interesting to study further this enhanced CR effect for the higher eigenmodes. This may be achieved, for example, by introducing multiple dipole inversion in the PI chains, one at the center ($n^* = N/2$) and the others at symmetrical locations with respect to the center ($n^* = n_1$ and $N - n_1$, etc). These inversions erase all dielectric contributions from the odd eigenmodes and tune the weight of $f_p(n)$ (p = even) in the dielectric intensities g_p. This will allow us to accurately determine $f_p(n)$ for higher even eigenmodes ($p = 4, 6, ...$). The synthesis and dielectric study of these new PI chains are an important subject of future work.

IV-2. Comparison of ΔF_p and τ_p Data with Models. The pure reptation and Rouse-type CR models, frequently used in the interpretation of dynamic data for entangled chains, commonly have sinusoidal eigenfunctions,[20,21,33]

$$f_p^{\circ}(n^*) = \sin(p\pi n^*/N) \tag{18a}$$

$$F_p^\circ(n^*) = (\sqrt{2}/p\pi)[1 - \cos(p\pi n^*/N)] \quad (18b)$$

The base-shifted eigenfunctions of the models, $F_p^\circ(n^*) = F_p^\circ(n^*) - F_p^\circ(N/2)$, are shown in Figure 6 with the dashed curves. The observed ΔF_p are nonsinusoidal and deviate from these F_p°.

One might suspect that the nonsinusoidal feature of ΔF_p may be an artifact due to uncertainties in our analysis. However, the same analysis yielded (almost) sinusoidal ΔF_p for the dipole-inverted PI chains in *dilute solutions* (at $c = 0.8c^*$),[10] as anticipated from coincidence[10] of their ϵ'' data with the ϵ'' calculated from the bead-spring model having the sinusoidal ΔF_p°. Thus, the nonsinusoidal feature of ΔF_p found for the PI chains in the blend and bulk systems (Figure 6) reflects the real nature of the chain dynamics in these environments.

This feature can be inferred also from the direct comparison of the normalized loss ($\epsilon''/\Delta\epsilon$) of I-I 49-0 with that calculated from the Rouse-CR/reptation models having the sinusoidal F_p°. At ω well-above ω_{peak}, both data and calculations exhibit the power-law behavior, $\epsilon''/\Delta\epsilon \propto \omega^{-\alpha}$, but the calculated exponent ($\alpha = {}^1/_2$) is significantly larger than the measured exponent ($\alpha \cong {}^1/_4$; see Figure 4). Since the integral $\int_{-\infty}^{\infty}[\epsilon''/\Delta\epsilon]\, d(\ln \omega)$ is equal to $\pi/2$ (due to the definition of $\Delta\epsilon$), this difference in the α values indicates that the measured $\epsilon''/\Delta\epsilon$ peak height h_ϵ is smaller than the height h_ϵ° obtained from the calculation. In fact, for I-I 49-0 (Figure 4), h_ϵ is $\cong$ 30% smaller than h_ϵ°; see also Figure 5 of Part 2.[31] (This difference is larger than an estimated uncertainty (<15%) in the measured h_ϵ and $\Delta\epsilon = (2/\pi)\int_{-\infty}^{\infty}\epsilon''(\omega)\, d(\ln \omega)$.)

For I-I 49-0 having no dipole inversion, both measured and calculated $\epsilon''/\Delta\epsilon$ peaks are dominated by a contribution from the slowest eigenmode and their heights h_ϵ and h_ϵ° are very close to $0.5\{F_1(N)\}^2$ and $0.5\{F_1^\circ(N)\}^2$, respectively (cf. eqs 10−12). Since F_p and F_p° are normalized so as to ensure the Gaussian nature of the chain (see Appendix), the 30% difference between h_ϵ and h_ϵ° unequivocally indicates the nonsinusoidal feature of F_1. (Note that h_ϵ is related to the *square* of $F_1(N)$ and modest differences between F_1 and F_1° are amplified when h_ϵ and h_ϵ° are compared.)

The nonsinusoidal feature of F_p indicates that the behavior of the I-I 49-0 chain is not accurately described by the Rouse-type CR and pure reptation models even for the two extreme cases where the CR mechanism makes either a negligible or a dominant contribution to the chain motion (in B263 or in B9). The corresponding failure of the pure reptation model is noted for viscoelastic moduli.[31]

The eigenfunction equation for the sinusoidal $f_p^\circ(n)$ coincides with the Schrödinger equation for a quantum particle in a square well potential (having the boundaries at $n = 0$ and N), and $[f_p^\circ(n)]^2$ is analogous to the probability density of this particle.[6,15] We may utilize this analogy and attribute the difference between $f_p^\circ(n)$ and $f_p(n)$ (between F_p and F_p°) to an additional potential near the well boundaries that decreases the probability density $[f_p(n)]^2$ near the boundaries.[6,15] This potential corresponds to a relaxation mechanism(s) not considered in the Rouse-type CR and reptation models. This extra mechanism enhances the relaxation near the chain ends to provide f_p (and F_p) with the nonsinusoidal feature. For the non-Rouse-type CR relaxation observed for dilute probes entangled with much shorter matrix chains, a previous study[15] suggested one possible mechanism enhancing the relaxation near the chain ends, contour-length variable local jumps. However, any mechanism giving this enhancement can yield the nonsinusoidal feature of f_p.[6,15] In other words, the origin of this feature is not necessarily identical for the two cases of CR-free and CR-dominant environments. Further theoretical studies are desirable to clarify this issue.

In contrast to the differences between ΔF_p and F_p° (Figure 6), the observed τ_p/τ_1 ratios (Table 3) are close to the ratios deduced from the pure reptation and Rouse-type CR models,

$$\tau_p/\tau_1 = p^{-2} \quad (19)$$

In particular, excellent agreement with the models is noted for I-I 49-0 in the CR-free B263 matrix. Thus, the above mechanism enhancing the relaxation near the chain ends hardly affects the relaxation time spacing deduced from the reptation and Rouse-type CR models.

IV-3. Meaning of CR-Insensitive Eigenmode Distribution. In general, the time evolution of the local correlation function $C(n,t;m)$ can be described by an equation of the form[17]

$$\frac{\partial}{\partial t}C(n,t;m) = L_C(n)\, C(n,t;m) \quad (20)$$

where $L_C(n)$ is an operator determined by the chain dynamics.[17,31] The solution of this equation, written in a form of an eigenmode expansion, is given by eq 4. The eigenfunctions $f_p(n)$ and relaxation times τ_p are determined by $L_C(n)$ through the equation,[17]

$$L_C(n)f_p(n) = -[1/\tau_p]f_p(n) \quad (21)$$

The functional form of $L_C(n)$ and the corresponding $f_p(n)$ and τ_p may differ for a given chain in different environments. However, *if* a proportionality $[L_C(n)]_1 = K[L_C(n)]_2$ (K = constant) holds for $L_C(n)$ in two environments 1 and 2, eq 21 results in a simple relationship for $[f_p(n)]_i$ and $[\tau_p]_i$ ($i = 1$ and 2) in these environments:

$$[f_p(n)]_1 = [f_p(n)]_2, \quad [\tau_p]_1 = K[\tau_p]_2 \quad (22)$$

For this case, the eigenmode distribution (characterized by $f_p(n)$ and the τ_p/τ_1 ratio) is the same in those environments.[38]

Experimentally, we have found that $f_p(n)$ and the τ_p/τ_1 ratio for the slowest three eigenmodes are nearly the same in the CR-free (B263) and CR-dominant (B9) matrices (Figures 6 and 7). This result suggests that the operator $L_C(n)$ for the actual, non-Rouse CR mechanism is nearly proportional to $L_C(n)$ for the other relaxation mechanism that is dominant in the high-M matrix and not relevant to the matrix diffusion. However, the differences in the higher eigenmodes in the two matrices indicate that the proportionality is only approximate.

It is important to note that the CR effect is quite different for dielectric and viscoelastic relaxation: In contrast to the behavior seen in Figure 4, changes in the CR contribution to the chain dynamics results in drastic changes in the viscoelastic mode distribution.[14,23,25,26,31] This reflects an essential difference between the local correlation function and the orientation function,[15,17,33] the former and latter respectively describing fundamental features of the dielectric and

viscoelastic relaxation processes. In Part 2,[31] we utilize this difference to examine detailed features (short-time coherence) of the chain motion.

V. Concluding Remarks

For the dipole-inverted PI chains in entangling matrices of various molecular weights, we have compared the dielectrically determined eigenfunctions $f_p(n)$ and relaxation times τ_p accompanying the local correlation function. For the slowest three eigenmodes, $f_p(n)$ and τ_p/τ_1 ratios are hardly affected by changes in the CR contribution to the chain motion. For higher eigenmodes, some CR effects are noted. In all matrices, $f_p(n)$ ($p = 1-3$) are nonsinusoidal with respect to the segment position n and deviate from the eigenfunctions deduced from the pure reptation and Rouse-type CR models, although the τ_p/τ_1 ratios are close to the model prediction. These results would provide an important starting point for refining molecular models that describe the dynamics of entangled chains in various environments.

Appendix. Characteristic Relationships for the Eigenfunctions.

The eigenfunctions $f_p(n)$ are determined by the operator L_C that reflects the feature of the chain dynamics (cf. eq 21). Thus, some relationships between the eigenfunctions of different order, $f_p(n)$ with $p = 1, 2, 3, ...$, are dependent on this feature and cannot be written in a general form. However, we can also find a relationship(s) that is valid irrespective of the chain dynamics, as explained below.

Normalization. In the blends and monodisperse bulk system examined in this study, the PI chains should have the Gaussian conformation. As noted from eqs 1 and 4, this conformation determines the initial condition of the local correlation function $C(n,t;m)$:

$$C(n,0;m) = \frac{2}{N}\sum_{p=1}^{N} f_p(n)\, f_p(m) = \delta_{nm} \qquad \text{(A1)}$$

Equation A1, indicating the equilibrium feature of the chain, specifies a relationship between the eigenfunctions that is valid irrespective of the chain dynamics. In particular, eq A1 holds for any set of eigenfunctions that are expanded in a form,

$$f_p(n) = \sum_{\alpha} a_{p\alpha} \sin(\alpha\pi n/N) \qquad \text{(A2)}$$

where $a_{p\alpha}$ are the components of a normalized, orthogonal matrix defined by

$$\sum_{\alpha} a_{p\alpha} a_{q\alpha} = \delta_{pq}, \quad \sum_{p} a_{p\alpha} a_{p\beta} = \delta_{\alpha\beta} \qquad \text{(A3)}$$

For f_p expanded in the form of eq A2, the coefficients $a_{p\alpha}$ reflect the feature of the operator L_C: Note that the Gaussian nature of the chain does not rule out the nonsinusoidal f_p (i.e., f_p having $a_{p\alpha} \neq \delta_{p\alpha}$ in eq A2.)

For the quantities we directly determined from the ϵ'' data, the integrated eigenfunctions $F_p(n)$ (eq 12), eq A1 is rewritten as

$$\sum_{p=1}^{N} F_p(n)\, F_p(m) = n/N \quad (\text{for} \quad n < m),\ m/N \quad (\text{for} \quad n > m) \qquad \text{(A4)}$$

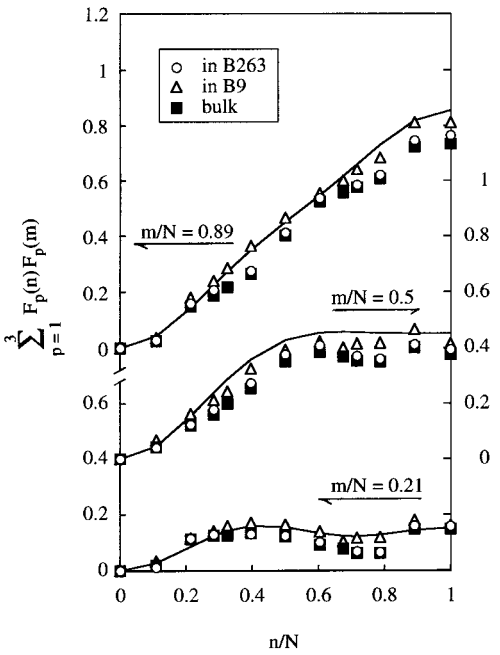

Figure A1. Plots of the sum $\sum_{p=1}^{3} F_p(n)\, F_p(m)$ for the I-I 49-0 chain in the three environments against the reduced segment position n/N. The plots are shown for representative m/N values. The solid curves indicate the sum calculated for the sinusoidal $F_p^{\circ}(n)$ with $p = 1-3$.

We evaluated the sum $\sum_{p=1}^{3} F_p(n)\, F_p(m)$ for our $F_p(n)$ data ($p = 1-3$) and examined the validity of eq A4. For some representative m/N values, the n/N dependence of this sum is shown in Figure A1. The solid curves indicate the sum calculated for the lowest three sinusoidal eigenfunctions, $F_p^{\circ}(n) = [\sqrt{2}/p\pi]\{1 - \cos[p\pi n/N]\}$ with $p = 1-3$.

The plots shown in Figure A1 are based only on the experimentally available F_p with $p = 1-3$. We do not expect that eq A4 holds rigorously for the data shown in Figure A1. However, these data qualitatively reproduce the characteristic feature of eq A4, the linear increase of the sum for $n < m$ and the leveling-off for $n > m$. In addition, we find good agreement of the data (in particular for the PI chains in B9) with the solid curves for the sinusoidal F_p° ($p = 1-3$). These results confirm the Gaussian nature of the PI chains.

Orthogonality. In general, the eigenfunctions f_p associating to the operator L_C (eq 21) are not necessarily orthogonal with each other. However, the orthogonality holds for any set of nonsinusoidal f_p given by eqs A2 and A3. We examine here whether the experimentally determined f_p also satisfies the orthogonal relationship (normalized according to eq 4),

$$I_{pq} = \frac{2}{N}\int_0^N f_p(n)\, f_q(n)\, \mathrm{d}n = \delta_{pq} \qquad \text{(A5)}$$

For this purpose, we numerically differentiate the $\Delta F_p(n)$ data for the I-I 49-0 chain in the blends and monodisperse bulk system (Figure 6) to evaluate $f_p(n) = [N/\sqrt{2}]\,[\mathrm{d}\Delta F_p(n)/\mathrm{d}n]$. This differentiation was carried out for curves smoothly connecting the ΔF_p data points in respective environments, and estimated uncertainties in this differentiation were less than 20%.

From the symmetry of f_p, $f_p(n) = f_p(N - n)$ for $p = 1$, 3 and $f_2(n) = -f_2(N-n)$, the integrals I_{pq} ($=I_{qp}$) automatically vanish for $[p,q] = [1,2]$ and $[2,3]$. The integrals for the other sets of $[p,q]$ are summarized in Table

Table A1. Second-Order Integrals[a] for Eigenfunctions of the I-I 49-0 Chain in Various Environments

	I_{11}	I_{13}	I_{22}	I_{33}
in B263	0.95	−0.18	0.74	1.29
in B9	1.04	−0.07	0.84	1.22
bulk	0.98	−0.17	0.73	1.08

[a] $I_{pq} = (2/N)\int_0^N f_p(n)\, f_q(n)\, dn$.

A1. We note that the $|I_{13}|$ is considerably smaller than I_{11} and I_{33} and the differences between I_{pq} and δ_{pq} are within the estimated uncertainties (less than 40% for the product $f_p f_q$). Thus, the orthogonality (eq A5) seems to be valid for the f_p data (although these uncertainties do not allow us to completely rule out some degree of nonorthogonal feature of f_p). This result is consistent with the form of eigenmode expansion for $C(n,t;m)$ (eq 4).

Finally, we have to emphasize that many operators L_C are associated with orthogonal eigenfunctions. Thus the orthogonality of the f_p data does not uniquely specify the functional form of L_C and the corresponding features of the chain dynamics.

References and Notes

(1) Imanishi, Y.; Adachi, K.; Kotaka, T. *J. Chem. Phys.* **1988**, *89*, 7585. See references therein for the earlier work on polydisperse PI chains.
(2) Adachi, K.; Yoshida, H.; Fukui, F.; Kotaka, T. *Macromolecules* **1990**, *23*, 3138.
(3) Yoshida, H.; Watanabe, H.; Adachi, K.; Kotaka, T. *Macromolecules* **1991**, *24*, 2981.
(4) Adachi, K.; Kotaka, T. *Prog. Polym. Sci.* **1993**, *18*, 585.
(5) Boese, D.; Kremer, F.; Fetters, L. J. *Macromolecules* **1990**, *23*, 829; Boese, D.; Kremer, F.; Fetters, L. J. *Macromolecules* **1990**, *23*, 1826.
(6) Watanabe, H.; Urakawa, O.; Kotaka, T. *Macromolecules* **1993**, *26*, 5073.
(7) Yoshida, H.; Adachi, K.; Watanabe, H.; Kotaka, T. *Polym. J. (Jpn.)* **1989**, *21*, 863.
(8) Patel, S. S.; Takahashi, K. M. *Macromolecules* **1992**, *25*, 4382.
(9) Urakawa, O.; Adachi, K.; Kotaka, T. *Macromolecules* **1993**, *26*, 2036; Urakawa, O.; Adachi, K.; Kotaka, T. *Macromolecules* **1993**, *26*, 2042.
(10) Watanabe, H.; Yamada, H.; Urakawa, O. *Macromolecules* **1995**, *28*, 6443.
(11) Urakawa, O.; Watanabe, H. *Macromolecules* **1997**, *30*, 652.
(12) Adachi, K.; Itoh, S.; Nishi, I.; Kotaka, T. *Macromolecules* **1990**, *23*, 2554.
(13) (a) Watanabe, H.; Yamazaki, M.; Yoshida, H.; Adachi, K.; Kotaka, T. *Macromolecules* **1991**, *24*, 5365. (b) Watanabe, H.; Yamazaki, M.; Yoshida, H.; Kotaka, T. *Macromolecules* **1991**, *24*, 5372.
(14) Watanabe, H.; Kotaka, T. *CHEMTRACTS Macromol. Chem.* **1991**, *2*, 139 and references therein.
(15) Watanabe, H.; Urakawa, O.; Kotaka, T. *Macromolecules* **1994**, *27*, 3525.
(16) Watanabe, H.; Urakawa, O.; Yamada, H.; Yao, M.-L. *Macromolecules* **1996**, *29*, 755.
(17) Watanabe, H.; Yao, M.-L.; Osaki, K. *Macromolecules* **1996**, *29*, 97.
(18) Equations 2 and 3 are derived for a Gaussian chain. For non-Gaussian chains, eqs 2 and 3 remain the same except that the prefactor $1/N$ is replaced by an appropriate normalization factor, $a^2/\langle \mathbf{R}^2 \rangle$.
(19) Klein, J. *Macromolecules* **1978**, *11*, 852.
(20) Graessley, W. W. *Adv. Polym. Sci.* **1982**, *47*, 67.
(21) Watanabe, H.; Tirrell, M. *Macromolecules* **1989**, *22*, 927.
(22) Watanabe, H.; Kotaka, T. *Macromolecules* **1984**, *17*, 2316.
(23) Watanabe, H.; Sakamoto, T.; Kotaka, T. *Macromolecules* **1985**, *18*, 1008; Watanabe, H.; Sakamoto, T.; Kotaka, T. *Macromolecules* **1985**, *18*, 1436.
(24) Watanabe, H.; Kotaka, T. *Macromolecules* **1986**, *19*, 2520.
(25) Watanabe, H.; Yoshida, H.; Kotaka, T. *Macromolecules* **1988**, *21*, 2175; Watanabe, H.; Yoshida, H.; Kotaka, T. *Macromolecules* **1992**, *25*, 2442.
(26) Watanabe, H.; Yamazaki, M.; Yoshida, H.; Kotaka, T. *Macromolecules* **1991**, *24*, 5573.
(27) Montfort, J.-P.; Marin, G.; Monge, P. *Macromolecules* **1984**, *17*, 1551.
(28) Montfort, J.-P.; Marin, G.; Monge, P. *Macromolecules* **1986**, *19*, 1979.
(29) Struglinski, M. J.; Graessley, W. W. *Macromolecules* **1985,** *18*, 2630.
(30) Struglinski, M. J.; Graessley, W. W.; Fetters, L. J. *Macromolecules* **1988**, *21*, 783.
(31) Watanabe, H.; Matsumiya, Y.; Osaki, K.; Yao, M.-L. *Macromolecules* **1998**, *31*, 7538.
(32) We compared plots of $\epsilon''/\Delta\epsilon$ against a reduced frequency $\omega\tau_1$ for the I14, I19, and I-I 49-0 chains in the B263 matrix. As noted for similar PI/PB blends,[13,14,16] the plots were indistinguishable and thus the dielectric mode distribution was universally scaled with the τ_1 shown in Figure 3. This result in turn indicates high accuracy of those τ_1 data.
(33) Doi, M.; Edwards, S. F. *The Theory of Polymer Dynamics*; Clarendon: Oxford, 1986.
(34) Ferry, J. D. *Viscoelastic Properties of Polymers*, 3rd ed.; Wiley: New York, 1980.
(35) Graessley, W. W. *Adv. Polym. Sci.* **1974**, *16*, 55.
(36) The coincidence of the shape of the ϵ'' curves for I-I 49-0 and I-I 24-24 was confirmed in each environment (B263, B9, and the monodisperse bulk system) from excellent superposition of the curves mutually shifted along the frequency axis.
(37) In principle, we can use ϵ'' data at higher ω to determine $g_p(n^*)$ for higher p (≥ 4). However, the τ_p spacing was too narrow for those p and the higher dielectric modes were not accurately resolved. Thus, as before,[6,10,15] we limited ourselves only to the determination of $g_p(n^*)$ for $p = 1-3$.
(38) A proportionality holds for the operators for the reptation and Rouse-type CR mechanisms, $L_C(n) = D[\partial^2/\partial n^2]$ with D being numerical coefficients for respective mechanisms.[21] Thus $f_p(n)$ and the τ_p/τ_1 ratio are the same for these mechanisms. This leads to the CR-independent dielectric mode distribution deduced from the configuration-dependent CR model.[21]

MA980055+